Dyes and Pigments 81 (2009) 144–151

Contents lists available at ScienceDirect

Dyes and Pigments

journal homepage: www.elsevier.com/locate/dyepig

1,4-Dithiaheterocycle-fused porphyrazines: Synthesis, characterization, voltammetric and spectroelectrochemical properties

Serap Tuncer [a], Atıf Koca [b], Ahmet Gül [c,*], Ulvi Avcıata [a,**]

[a] Department of Chemistry, Yildiz Technical University, Davutpasa 34210, Istanbul, Turkey
[b] Chemical Engineering Department, Engineering Faculty, Marmara University, Kadıköy, Istanbul, Turkey
[c] Department of Chemistry, Technical University of Istanbul, Maslak 34469, Istanbul, Turkey

ARTICLE INFO

Article history:
Received 26 May 2008
Received in revised form 26 September 2008
Accepted 30 September 2008
Available online 14 October 2008

Keywords:
Porphyrazines
Phthalocyanines
Magnesium
Cobalt
Zinc
Electrochemistry
Cyclic voltammetry
Spectroelectrochemistry

ABSTRACT

Porphyrazines (M = H, Mg, Zn and Co) with a 2,3-dicyano-5-phenyl-5,6-dihydro-1,4-dithiin group fused to each pyrrole unit were synthesized and characterized starting with the corresponding unsaturated dicarbonitrile derivative. The voltammetric and spectroelectrochemical characterizations of the metallo-porphyrazines (M = $2H^+$, Mg^{2+}, Zn^{2+} and Co^{2+}) substituted with 2,3-dicyano-5-phenyl-5,6-dihydro-1,4-dithiin groups on peripheral positions are described. Cyclic voltammetry and differential pulse voltammetry studies showed that while metal-free, magnesium, and zinc porphyrazines represented well-defined one-electron ligand-based reductions and ligand-based one-electron oxidation couples, cobalt porphyrazine gave both metal-based and ligand-based reduction and oxidation couples. Assignments of the redox couples were confirmed by spectroelectrochemical measurements.

1. Introduction

Tetrapyrrole macrocycles such as phthalocyanines, porphyrines and porphyrazines have been of great scientific interest for their widespread applications in areas such as coloring materials – pigment, energy conversion, electrophotography, gas sensors, liquid crystals, infrared dyes for laser technology and optical data storage. They have also been of considerable interest to theoretical chemists owing to their high symmetry, planarity, thermal stability and electronic delocalization [1,2]. A significant amount of work has been carried out on their magnetic and catalytic properties and also on their role in biomolecular processes [3,4].

In recent times, porphyrazines have gained more attention due to the simplistic nature of their synthesis via the cyclotetramerisation of maleonitrile [5]. During the last decade, we have been heavily engaged with the preparation of new porphyrazines in parallel with phthalocyanine analogues [6–10]. Substitution of various groups (e.g., dimethylaminoethylthio- [11], tosylaminoethylthio- [12], etc.) on the peripheral positions of porphyrazines has been accomplished by either starting with an unsaturated dinitrile precursor or a preformed porphyrazine with reactive functional groups that can be subsequently modified (e.g., ferrocene [13], benzo-15-crown-5 [14], pyridine [8], 1,4-dithiahexene- [7], etc. have been incorporated by further condensation reactions).

Compared to the more intensely studied works on the synthesis and electrochemistry of phthalocyanines [15–17], related work on, especially the spectroelectrochemical investigation of porphyrazines, has been scarce [18–20]. Thus in the present paper we report the preparation of porphyrazine macrocycles having 2,3-dicyano-5-phenyl-5,6-dihydro-1,4-dithiin units annulated to the pyrrole groups and we have examined the electrochemical and spectroelectrochemical properties of these compounds. Voltammetric and spectroelectrochemical characterizations of the complexes are important for the insight of the their possible technological application especially in the electrochromic and electrocatalytic fields.

2. Experimental

2.1. Reagents, instruments and measurements

The starting compound, styrene dibromide was purchased from Fluka Company. All reagents and solvents were of reagent grade

* Corresponding author. Tel.: +90 212 285 68 27; fax: +90 212 285 63 86.
** Corresponding author. Tel.: +0212 4491890; fax: +0212 4491888.
E-mail addresses: ahmetg@itu.edu.tr (A. Gül), uavciata@yildiz.edu.tr (U. Avcıata).

0143-7208/$ – see front matter © 2008 Elsevier Ltd. All rights reserved.
doi:10.1016/j.dyepig.2008.09.022

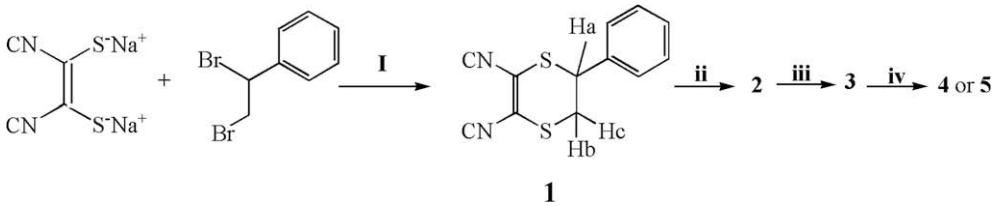

Scheme 1. Synthesis scheme for the new products **1**–**5**. (i) DME, 85 °C, 24 h; (ii) $Mg(BuO)_2$, BuOH, 120 °C; (iii) CF_3COOH, r.t.; (iv) $Zn(OAc)_2$, THF, EtOH in the case of **4** or $Co(OAc)_2$, THF, EtOH in the case of **5**.

quality and were obtained from commercial suppliers. The starting compound, dithiomaleonitrile disodium salt was prepared according to the reported procedure [21,23]. The purity of the products was tested in each step by TLC (SiO_2). IR spectra were recorded on a Mattson 1000 FTIR spectrophotometer using KBr pallets, electronics absorption spectra on an Agilent 8453 UV–vis spectrophotometer. Elemental analyses were carried out using Slashea 1112 Serie Thermo. ^{1}H NMR spectra were recorded on a Bruker 250 MHz.

The cyclic voltammetry (CV), differential pulse voltammetry (DPV), and double potential step coulometry (DPSC) measurements were carried out with Gamry Reference 600 potentiostat/galvanostat controlled by an external PC and utilizing a three-electrode configuration at 25 °C. The working electrode was a Pt disc with a surface area of 0.071 cm^2. The surface of the working electrode was polished with a diamond suspension before each run. A Pt wire served as the counter electrode. Saturated calomel electrode (SCE) was employed as the reference electrode and separated from the bulk of the solution by a double bridge. Ferrocene was used as an internal reference. Electrochemical grade tetrabutylammonium perchlorate (TBAP) in extra pure dichloromethane (DCM) was employed as the supporting electrolyte at a concentration of 0.10 mol dm^{-3}. High purity N_2 was used to remove dissolved O_2 at least 15 min prior to each run and to maintain a nitrogen blanket during the measurements. IR compensation was also applied to the CV scans to minimize the potential control error.

The spectroelectrochemical measurements were carried out with an Ocean-optics QE65000 diode array spectrophotometer equipped with the potentiostat/galvanostat utilizing a three-electrode configuration of thin-layer quartz spectroelectrochemical cell at 25 °C. The working electrode was Pt tulle. Pt wire counter electrode separated by a glass bridge and a SCE reference electrode separated from the bulk of the solution by a double bridge were used.

2.2. Synthesis

2.2.1. Synthesis of 2,3-dicyano-5-phenyl-5,6-dihydro-[1,4] dithiin (*1*)

A mixture of styrene dibromide (5.30 g, 0.020 mol) and dithiomaleonitrile disodium salt (5.20 g, 0.028 mol) was heated at 85 °C under reflux with stirring in dimethyl ether (DME) (50.0 mL) for 24 h. Then the cooled mixture was poured into water, filtered and the solid product was washed well with water. The dried solid was extracted with three 25.0 mL portions of hot carbon tetrachloride. Finally, the combined extracts were deposited as crystals on evaporation *in vacuo*. Yield: 0.8 g, 16.5%. Mp 124–125 °C. Anal. Calc. for $C_{12}H_8N_2S_2$: C, 58.98; H, 3.28; N, 11.46; S, 26.24. Found: C, 57.59; H, 3.15; N, 11.41; S, 26.19%. IR (KBr), υ (cm^{-1}): 2980, 2953, 2876, 2212, 1523, 1472, 1165, 1140, 1038, 881, 757, 706, 520. ^{1}H NMR (*d*-chloroform, 250 MHz): 3.43–3.46 (dd, $J = 4.7$ and 6.9 Hz, 2H, Hb, Hc), 4.54–4.58 (dd, $J = 4.7$ and 6.9 Hz, 1H, Ha), 7.24–7.45 (m, aromatic).

2.2.2. Synthesis of tetrakis-[5-phenyl-5,6-dihydro-[1,4] dithiino]porphyrazinato magnesium (*2*)

Mg powder (22.0 mg, 0.905 mmol) was dissolved by refluxing overnight in BuOH (18.0 mL) with addition of a few crystals of I_2 at 120 °C. To this magnesium butoxide suspension, **1** (400.0 mg, 1.637 mmol) was added. After refluxing for 24 h under N_2 at 120 °C, a dark blue suspension was obtained. Then the mixture was filtered while it was hot. Finally, the crude residue was washed first with BuOH and then with methanol and finally with *n*-hexane and dried *in vacuo*. Yield: 283 mg, 70%. Anal. Calc. for $C_{48}H_{32}N_8S_8Mg$: C, 57.55; H, 3.22; N, 11.18; S, 25.61. Found: C, 56.85; H, 3.15; N, 11.35; S, 24.84%. IR (KBr), υ (cm^{-1}): 2957, 1592, 1531, 1445, 1049, 696. ^{1}H NMR (*d*-chloroform, 250 MHz): 3.43–3.46 (br s, 4H, Ha); 3.69–3.71 (d, $J = 6.3$ Hz, 8H, Hb, Hc); 7.31–7.56 (m, aromatic). UV–vis λ_{max} (nm) (log ϵ) in $CHCl_3$: 669 (4.84), 618 (4.34), 371 (4.81).

2.2.3. Synthesis of tetrakis-[5-phenyl-5,6-dihydro-[1,4] dithiino] porphyrazine (*3*)

Compound **2** (200.0 mg, 0.199 mmol) was demetallised by treatment with CF_3COOH (highly corrosive; avoid contact with water; 5.0 mL) at room temperature for 24 h and then the mixture was added dropwise into ice water. The medium was neutralized with ammonia solution (25% aq.). Finally, it was filtered, washed first with water, then with MeOH and finally with diethylether and dried *in vacuo*. Yield: 115 mg, 58%. Anal. Calc. for $C_{48}H_{34}N_8S_8$: C, 58.99; H, 3.26; N, 11.43; S, 25.14. Found: C, 57.90; H, 3.21; N, 10.97; S, 24.01%. IR (KBr), υ (cm^{-1}): 3300, 2957, 1488, 1312, 1036, 872, 736,

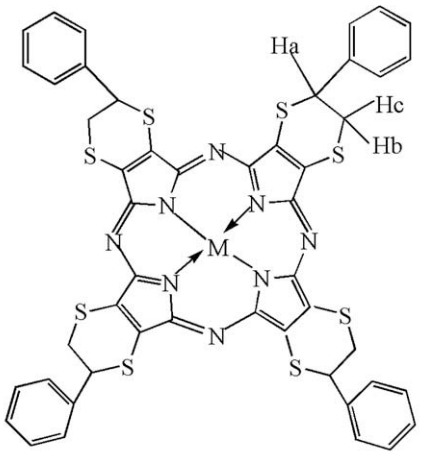

	2	3	4	5
M	Mg^{2+}	$2H^+$	Zn^{2+}	Co^{2+}
MPz	MgPz	H_2Pz	ZnPz	CoPz

Scheme 2. Porphyrazine molecule and their derivatives.

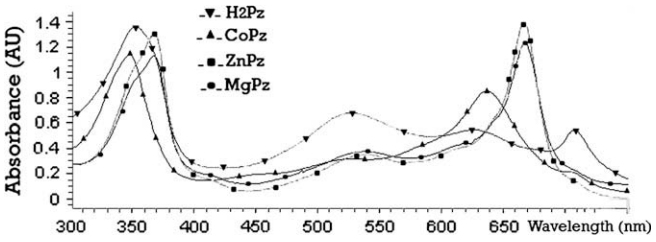

Fig. 1. UV–vis absorption spectra of porphyrazine derivatives in $CHCl_3$.

695. ^{1}H NMR (*d*-chloroform, 250 MHz): 4.98 (br s, 4H, Ha); 3.63–3.84 (br s, 8H, Hb, Hc); 7.32–7.33 (m, aromatic); 7.53 (br s, aromatic). UV–vis λ_{max} (nm) (log ϵ) in $CHCl_3$: 707 (4.49), 521 (4.47), 351 (4.13).

*2.2.4. Synthesis of tetrakis-(5-phenyl-5,6-dihydro-[1,4] dithiino)-porphyrazinato zinc (**4**)*

Compound **3** (50.0 mg, 0.051 mmol) in THF (10.0 mL) was refluxed with $Zn(OAc)_2$ (25.0 mg, 0.112 mmol) in EtOH (10.0 mL) for 24 h. After filtration, the filtrate was evaporated to dryness. Finally, the crude product was washed successively with hot water, MeOH and *n*-hexane and then dried *in vacuo*. Yield: 28 mg, 56%. Anal. Calc. for $C_{48}H_{32}N_8S_8Zn$: C, 55.13; H, 3.06; N, 10.72; S, 24.50. Found: C, 54.90; H, 2.99; N, 10.51; S, 24.25%. IR (KBr), υ (cm^{-1}): 2923, 2853, 1631, 1451, 1290, 1051, 801, 696. ^{1}H NMR (*d*-chloroform, 250 MHz): 3.59–3.68 (br s, 4H, Ha); 3.68–3.88 (br s, 8H, Hb, Hc); 7.31–7.56 (m, aromatic). UV–vis λ_{max} (nm) (log ϵ) in THF: 666 (4.78), 619 (4.27), 366 (4.80).

*2.2.5. Synthesis of tetrakis-(5-phenyl-5,6-dihydro-[1,4] dithiino)-porphyrazinato cobalt (**5**)*

To obtain **5**, same procedure for the synthesis of **4** was applied by starting with **3** (50.0 mg, 0.051 mmol) and $Co(OAc)_2$ (25.0 mg, 0.102 mmol). Yield: 25 mg, 50%. Anal. Calc. for $C_{48}H_{32}N_8S_8Co$: C, 55.47; H, 3.08; N, 10.78; S, 24.65. Found: C, 54.38; H, 3.10; N, 10.30; S, 23.53%. IR (KBr), υ (cm^{-1}): 2919, 2846, 1665, 1489, 1264, 1065, 1035, 871, 794, 737, 696. UV–vis λ_{max} (nm) (log ϵ) in THF: 635 (4.70), 525 (5.05), 346 (4.55).

3. Results and discussion

3.1. Synthesis and characterization

As in the case of almost all synthetic procedures leading to porphyrazines, we need to start with unsaturated 1,2-dinitriles with heterocyclic units directly fused to these functional groups. Among many compounds which might be considered in this context, a dithiin derivative, namely 2,3-dicyano-5-phenyl-5,6-dihydro-[1,4] dithiin has been preferred and the reaction to obtain the compound was reported in detail by Simmons et al. [22,23]. Essentially, the disodium salt of dithiomaleonitrile was first converted to an intermediate with addition of styrene dibromide. The styrene dibromide was used to obtain **1** in DME. The product yield was 16.5% (Scheme 1).

The cyclotetramerisation process with dinitrile derivative, **1** in the presence of magnesium butanolate was observed to be the only way to synthesize the magnesium porphyrazinate derivative, **2**, in butanol (Scheme 2). Treatment of this magnesium compound with a strong organic acid, e.g., trifluoroacetic acid, at room temperature for 24 h afforded the metal-free derivative **3**.

Table 1
Voltammetric data of the complexes with the related lead phthalocyanines for comparison.

Complex		Redox processes					$\Delta E_{1/2}$[d]	Reference
		O_2	O_1	R_1	R_2	R_3		
MgPz (**2**)	$E_{1/2}$[a] (V vs. SCE)	1.52[e]	1.10	−0.71	−1.10	−1.85[e]	1.81	
	ΔE_p[b] (mV)	106	115	63	87	–		tw
	I_{pa}/I_{pc}[c]	–	1.00	0.96	0.95	–		
H_2Pz (**3**)	$E_{1/2}$[a] (V vs. SCE)		1.07	−0.47	−0.77	−1.72[e]	1.54	
	ΔE_p[b] (mV)			58	63	85		tw
	I_{pa}/I_{pc}[c]			0.30	0.90	–		
ZnPz (**4**)	$E_{1/2}$[a] (V vs. SCE)	–	0.98	−0.47	−0.91		1.45	
	ΔE_p[b] (mV)							tw
	I_{pa}/I_{pc}[c]							
CoPz (**5**)	$E_{1/2}$[a] (V vs. SCE)	1.60[e]	0.63	−0.12	−1.07	−1.74	0.75	
	ΔE_p[b] (mV)			88	84	120		tw
	I_{pa}/I_{pc}[c]							
H_2Pz[f]	$E_{1/2}$ (SCE) in THF			−0.10	−0.46	−1.20		[29]
H_2Pz[g]	$E_{1/2}$ (SCE) in DCM	1.09	0.90	−0.21	−0.50	−0.91		[30]
H_2Pz[h]	$E_{1/2}$ (SCE) in DCM			−0.37	−0.78	−1.20		[7]
H_2Pz[i]	$E_{1/2}$ (SCE) in DCM		1.41	−0.28	−0.65	−1.56		[27]
CoPz[g]	$E_{1/2}$ (SCE) in DCM	1.14	0.70	−0.10	−0.36	−1.04		[30]
CoPz[i]	$E_{1/2}$ (SCE) in DCM		1.42	−0.28	−0.62	−1.60		[27]
CuPz[g]	$E_{1/2}$ (SCE) in DCM		0.62	−0.09	−0.43	−1.32		[30]
ZnPz[h]	$E_{1/2}$ (SCE) in DCM			−0.63	−1.03	−1.31		[7]
ZnPz[i]	$E_{1/2}$ (SCE) in DCM	1.32	0.74	−0.38	−0.72	−1.62		[27]
MgPz[i]	$E_{1/2}$ (SCE) in DCM		1.15	−0.52	−0.87			[27]

tw: this work.
[a] $E_{1/2} = (E_{pa} + E_{pc})/2$ at 0.100 V s^{-1} (E_{pc} for reduction, E_{pa} for oxidation for irreversible processes).
[b] $\Delta E_p = E_{pa} - E_{pc}$ at 0.100 V s^{-1} scan rate.
[c] I_{pa}/I_{pc} for reduction, I_{pc}/I_{pa} for oxidation processes at 0.100 V s^{-1} scan rate.
[d] $\Delta E_{1/2} = \Delta E_{1/2}$ (first oxidation) − $\Delta E_{1/2}$ (first reduction) = HOMO–LUMO gap for metal-free and metallo-porphyrazines having electro-inactive metal center (metal to ligand (MLCT) or ligand to metal (LMCT) charge transfer transition gap for MPz having redox active metal center.).
[e] Recorded by differential pulse voltammetry.
[f] Substituted with octakis-tosylaminoethylthio groups.
[g] Substituted with octakis –crown ether groups.
[h] Substituted with tetrakis-[(6,7,8,8a-tetrahydro-4a*H*-[1,4] dithiino-[2,3-*b*]pyrano)] groups.
[i] Substituted with eight (1-naphthylmethylthio) groups.

Apparent differences between magnesium and metal-free derivative are the change of color from dark blue to purple blue and lowering the solubility. Insertion of metal ions into metal-free derivative has been proven to be the only route to further metallize these macrocycles [24]. A range of conditions for the conversion of metal-free porphyrazine, **3** into cobalt and zinc complexes were investigated [11–14,25].

FTIR spectra clearly indicated the presence of the proposed functional groups at 2980, 2953, 2876 (CH), and 2212 cm^{-1} (CN) as intense absorptions. Cyclotetramerisation of the dinitriles was confirmed by the disappearance of the sharp C≡N vibration at 2212 cm^{-1} present in **1**. The NH groups in the inner core of the metal-free derivative, **3**, gave an absorption peak at 3300 cm^{-1} [13,14]. In the ^1H NMR of compound **1**, CH proton appeared at the lower field as a doublet of doublet at 4.54–4.58 and CH_2 protons resonate at 3.43–3.46 ppm. The benzene protons appear as a multiplet at 7.24–7.45 ppm. The most revealing data for a tetrapyrrole system are given by their UV–vis spectra in solution (Fig. 1). Compound **3** exhibited a split in Q-band absorption which is due to π–π^* transitions of these completely conjugated 18-π electron systems. The consequence of the lower symmetry introduced by variations of the substituents on the periphery was hardly observed as a shoulder at the lower energy side of the intense Q-bands, so the characteristic Q-band transitions of the metal porphyrazinates were observed as a single band of high intensity. The effect of eight S-substituents on the periphery of the porphyrazine core was a shift in these intense Q-bands to longer wavelengths when compared with those of unsubstituted or alkyl substituted derivatives [26]. Sometimes, the peripheral positions of substituted groups are in uncertain position, the asymmetrically substituted dithiin derivatives could be synthesized but these isomers only have very small effect on the spectroscopic characterization data. Isomers may cause broadening of the bands recorded in the UV–vis and especially in the IR spectra.

3.2. Voltammetric and spectroelectrochemical measurements

The solution redox properties of the complexes were studied using cyclic voltammetry (CV), differential pulse voltammetry (DPV), and controlled potential coulometry (CPC) in DCM on a platinum electrode. Table 1 lists the redox potentials of the complexes with the related porphyrazines data from the literature for comparison. The redox potentials of the complexes shift toward negative potentials with respect to common porphyrazine derivatives due to the effect of electron releasing 2,3-dicyano-5-phenyl-5,6-dihydro-1,4-dithiin moieties [7,19,20,27–31]. The separation between the first ring reduction and the first ring oxidation processes ($\Delta E_{1/2}$) related with the HOMO–LUMO gap for metal-free porphyrazines and metallo-porphyrazines having redox inactive metal center and the peak-to-peak separations are in agreement with the reported separation for redox processes in porphyrazine derivatives. The separation between the first ring reduction and first ring oxidation for cobalt porphyrazine (**5**) is lesser than others due to the electroactive central metal [7,19,20,27–31].

Fig. 2 shows typical cyclic (CV) and differential pulse (DPV) voltammograms of **3**. One oxidation process labeled as O_1 at 1.07 V and three reduction processes labeled as R_1, R_2, and R_3 at −0.47, −0.77 and −1.7 V vs. SCE at 0.100 V s^{-1} scan rate are observed within the potential window of electrolyte system. For the couples (R_1 and R_2), anodic to cathodic peak separation (ΔE_p) changed from 56 to 105 V with the scan rates ranging from 0.010 to 0.500 V s^{-1} (60–110 mV was obtained for ferrocene) suggesting reversible electron transfer characteristics of the processes. Moreover reversibility is illustrated by the similarity in the forward and reverse DPV scans (Fig. 2B) [32,33]. Wider potential window could be scanned with DPV than those of CV, thus the third reduction process could be recorded with DPV while only first two reduction processes recorded with CV measurements. The peak currents increased linearly with the square root of scan rates, for scan rates ranging from 0.010 to 0.500 V s^{-1}, indicating that the electrode reactions are purely diffusion controlled for the couples R_1 and R_2 [32,33]. The values of I_{pa}/I_{pc} for these couples of the compound are close to unity, supporting purely diffusion controlled mass transfer of the compound.

Complexes **2** (Fig. 3) and **4** (Fig. 4) give similar voltammetric behavior with **3** accompanied by the significant potential shifts corresponding to the different metal centers of the complexes (Table 1). While two reductions and one oxidation redox couples with **2** are recorded during CV measurements, an extra oxidation couple (O_2) at 1.52 V is recorded with DPV due to the wider potential windows of the DPV. Complex **4** gives three reduction and one oxidation redox processes within the potential windows of the DCM/TBAP electrolyte system. Voltammetric measurements confirm the aggregation–disaggregation equilibrium of **4** by splitting the reduction and oxidation peaks of the complex. Diluting the solution decreases the wave assigned to the aggregated species more than the waves assigned to the monomeric ones. This behavior supports the existence of the aggregation–disaggregation equilibria. Aggregation of the complex exists even at much diluted solution ($\sim 10^{-5}$ mol dm^{-3}) as shown in the UV–vis spectra in Fig. 5 (broadening of the Q-band and shoulder of the Q-band show the aggregation). Aggregation state of the complex also will be discussed below observed with spectroelectrochemical measurements.

Compounds **2**–**4**, have all redox inactive metal centers. Therefore, in situ UV–vis spectral changes of **4** are given as

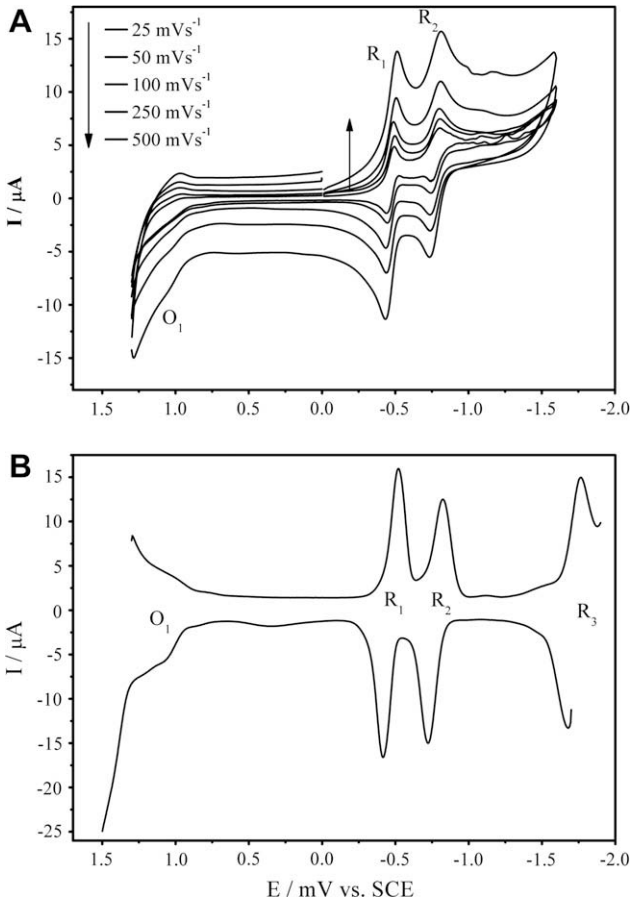

Fig. 2. (A) CVs and (B) DPVs of **3** at various scan rates on Pt in DCM/TBAP (pulse time: 50 ms, pulse size: 100 mV, step size: 5 mV, sample period: 100 ms).

a representative of the spectral changes of MPz having redox inactive metal center. As shown in Fig. 5, there are two distinct spectroscopic changes, which are recorded during the potential applications at the first reduction process of the complex **4**. First of all, while the intensity of Q-band at 664 nm increases without shift, the band at 540 nm assigned to the aggregated species decreases in intensity (Fig. 5A). These changes support the aggregation–disaggregation equilibrium of **4** recorded in CV of the complex. Then as shown in Fig. 5B, the intensity of Q-band at 664 nm decreases without shift and new bands in the MLCT regions at 450, 550 and 850 nm are recorded. Decrease in the intensity of Q-band without shift and observation of new bands in the MLCT regions are characteristics of ring-based processes. Color change from blue to red supports the generation of monoanionic $[Zn(II)Pz(-3)]^{-1}$ species during the process. Fig. 5C shows the ligand-based oxidation processes of the complex under the potential application at 1.0 V. The band formation at 435, 540 and 787 nm and decrease of the Q-band in intensity without shift indicate the formation of $[Zn(II)Pz(-1)]^{+}$ species, confirming the CV assignment of couple O_1 to ligand-based oxidation process [19,20,27–29,34–37].

Fig. 6 represents the CV and DPV of complex **5**. Within the potential windows, two oxidation process labeled as O_1 and O_2 and three reduction processes labeled as R_1, R_2, and R_3 at 0.63, 1.60, −0.12, −1.07 and −1.74 V vs. SCE at 0.100 V s^{-1} scan rate, respectively, are observed. The first one-electron reduction of [Co(II)Pz] in DCM occurs at an $E_{1/2}$ value slightly less negative than the first reduction processes of the complexes examined above (Table 1), whereas the first oxidation occur at less positive values. For the first oxidation process of the CoPz and CoPc complexes, values of potentials and site of oxidation are both strongly solvent and electrolyte-dependent. In a noncoordinating solvent such as DCM, the first oxidation of Co(II)Pz is assigned as ligand-centered, but a ring-centered oxidation has been observed in dry noncoordinating solvents such as DMSO containing weakly coordinating anions. In coordinating solvents, axial ligation at the metal center stabilizes Co(III) and hence the oxidation of Co(II)Pz and Co(II)Pc is metal-centered and occurs at markedly lower potentials than in noncoordinating solvents [18]. According to these studies, the first oxidation of Co(II)Pz recorded here at 0.63 V is assumed to be ligand-centered. The first reduction at −0.12 V is assigned as the $[Co(II)\ Pz(-2)]/[Co(I)\ Pz(-2)]^{1-}$ process and the second and third reductions as ligand-centered reductions on the basis of results in the literature. All predicted redox processes are given in Eq. (1). The nature of the redox couples will be also confirmed below using spectroelectrochemistry measurements. The separation between the metal center reduction and the ring oxidation processes (0.87 V) is comparable with the Co(II)Pz papers [18].

$$\begin{aligned}&[Co(II)Pz(-1)]^{1+} \overset{-e^-}{\underset{O_2}{\Leftrightarrow}} [Co(III)Pz(-1)]^{2+}\\ &\quad -e^- \Updownarrow O_1\\ &[Co(II)Pz(-2)]\\ &\quad +e^- \Updownarrow R_1\\ &[Co(I)Pz(-2)]^{1-} \overset{+e^-}{\underset{R_2}{\Leftrightarrow}} [Co(I)Pz(-3)]^{2+} \overset{+e^-}{\underset{R_3}{\Leftrightarrow}} [Co(I)Pz(-4)]^{3-}\end{aligned} \quad (1)$$

Spectroelectrochemical studies were employed to confirm the assignments in the CVs of **5**. Fig. 7A shows the UV–vis spectral changes during a controlled potential reduction of **5** at −0.03 V vs.

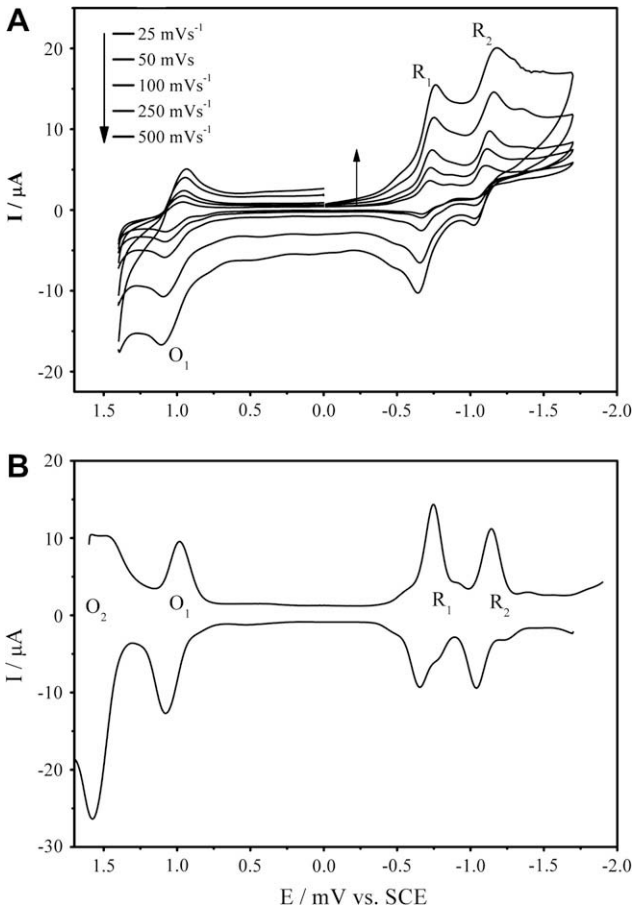

Fig. 3. (A) CVs and (B) DPVs of **2** at various scan rates on Pt in DCM/TBAP (pulse time: 50 ms, pulse size: 100 mV, step size: 5 mV, sample period: 100 ms).

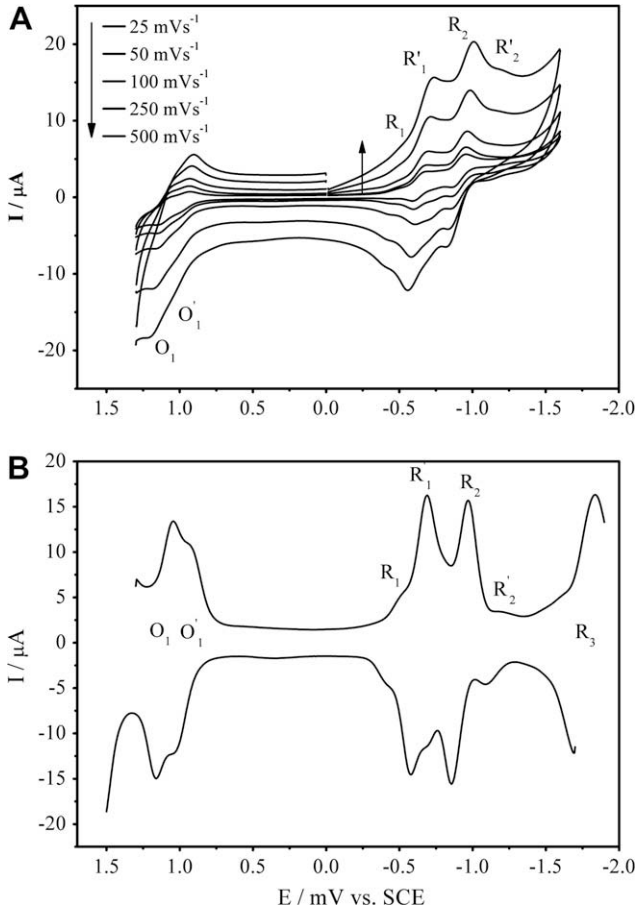

Fig. 4. (A) CVs and (B) DPVs of **4** at various scan rates on Pt in DCM/TBAP (pulse time: 50 ms, pulse size: 100 mV, step size: 5 mV, sample period: 100 ms).

SCE corresponding to the redox process labeled as R_1 in the CV. The starting spectrum compared to Fig. 1 is broader due to the existence of TBAP in solution. Absorption of the Q-band increases slightly with shift from 630 nm to 665 nm while the B-band shifts from 335 to 310 nm. Two new bands at 445 and 560 nm in the metal to ligand charge transfer (MLCT) region appear as the reduction process continued. The band formation at 445 nm and shifting of the Q-band indicate the formation of $[Co(I)Pz(-2)]^-$ species, confirming the CV assignment of couple R_1 to $[Co(II)Pz(-2)]/[Co(I)Pz(-2)]^-$ process [7,19,20,27–29,31–37]. This process results with clear isosbestic points at 325, 367, 500, 530, 590, 645 and 725 nm in the spectra. Color change from purple to red supports the generation of monoanionic $[Co(I)Pz(-2)]^-$ species during the process. The spectral changes in Fig. 7B are typical of ring-based reduction in porphyrazine complexes. Decreases in the intensity of the band at 380 nm and Q-band at 665 nm without shift and increases in the region at around 500 nm upon further reduction of the $[Co(I)Pz(-2)]^-$ species at potentials of couple R_2 were recorded as shown in Fig. 7B [7,19,20,27–29,31–37]. This confirms our earlier assignment of the process labeled R_2 to $[Co(I)Pz(-2)]^-/[Co(I)Pz(-3)]^{2-}$. Fig. 7C shows the spectral changes observed when the potential corresponding to the process O_1 was applied to the solution of $[Co(II)Pz(-2)]$. The Q-band absorption at 665 nm increases without shift while the B-band increases with shift from 340 to 360 nm. Increase in intensity of the Q-band is due to the aggregation–disaggregation equilibrium of the species. Change in the absorption of the Q-band without shift is typical of ligand-based oxidation in Co(II)Pz complexes. The final spectrum in Fig. 7C is therefore assigned to $[Co(II)Pz(-1)]^+$ species, confirming CV assignments. This process is resulted with clear isosbestic points at 348, 423 and 540 nm in the spectra. As shown in Fig. 7D, further oxidation shows the oxidation of $[Co(II)Pz(-1)]^+$ species to$[Co(III)Pz(-1)]^{2+}$ species. Red shift of the Q-band from 665 nm to 692 nm and observation of a new band at 440 nm are characteristic of a metal-based oxidation process and confirm the CV assignments of the O_2 process to $[Co(II)Pz(-1)]^+/[Co(III)Pz(-1)]^{2+}$ redox couple. *I* the intensity of the band at 550 nm is due to the disaggregation of the aggregated species. This process is resulted with clear isosbestic points at 385, 478 and 678 nm.

The CPC studies indicated that the number of electrons transferred for the first reduction processes of the complexes was found approximately one. Since both reduction processes have very similar peak currents, the number of electrons transferred for the remaining processes should also be one. To obtain a more accurate measurement of the redox equivalency, reduction processes were studied by DPSC. Plots of *Q* (charge) versus $t^{1/2}$ (time) show a linear behavior for both first two reduction processes. Slopes with a 1:1 ratio were consistent with the involvement of one-electron transfer for R_1 and R_2 processes of the complexes. DPSC experiments also

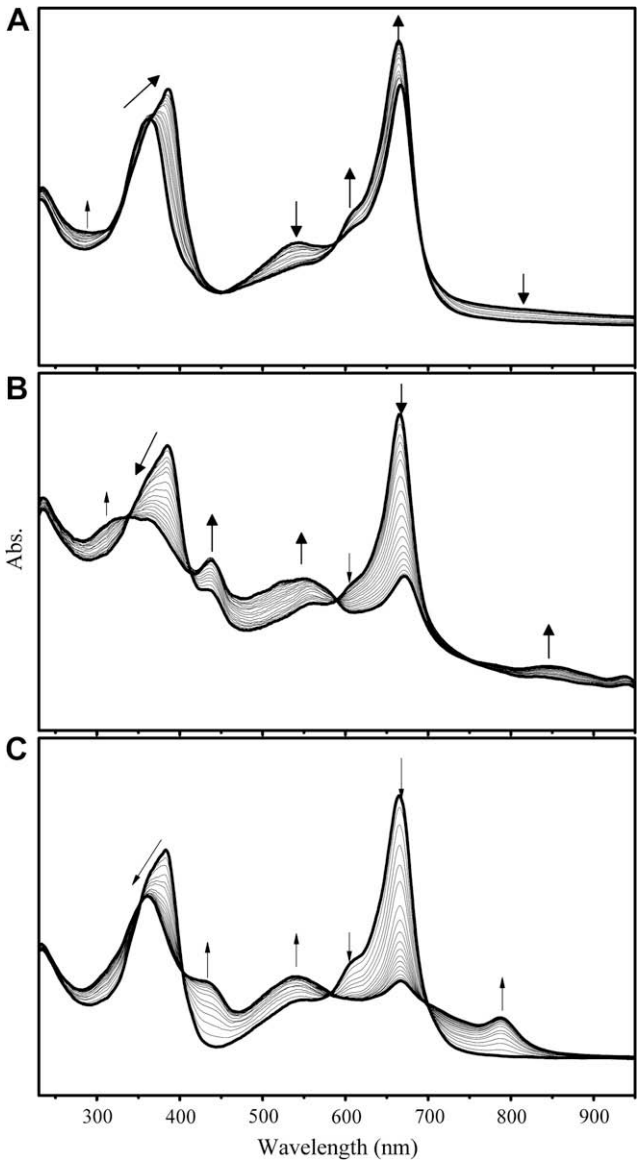

Fig. 5. In situ UV–vis spectral changes of **4**. (A) First part of the spectral changes recorded at potential application, $E_{app} = -0.70$ V; (B) last part of the spectral changes recorded at potential application, $E_{app} = -0.70$ V; (C) $E_{app} = 1.20$ V.

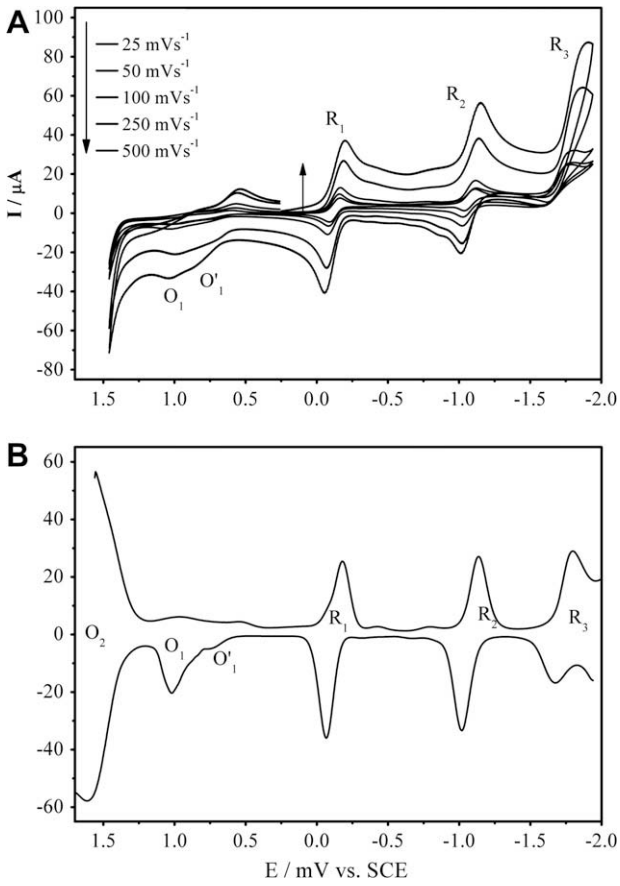

Fig. 6. (A) CV and (B) DPV of **5** at various scan rates on Pt in DCM/TBAP (pulse time: 50 ms, pulse size: 100 mV, step size: 5 mV, sample period: 100 ms).

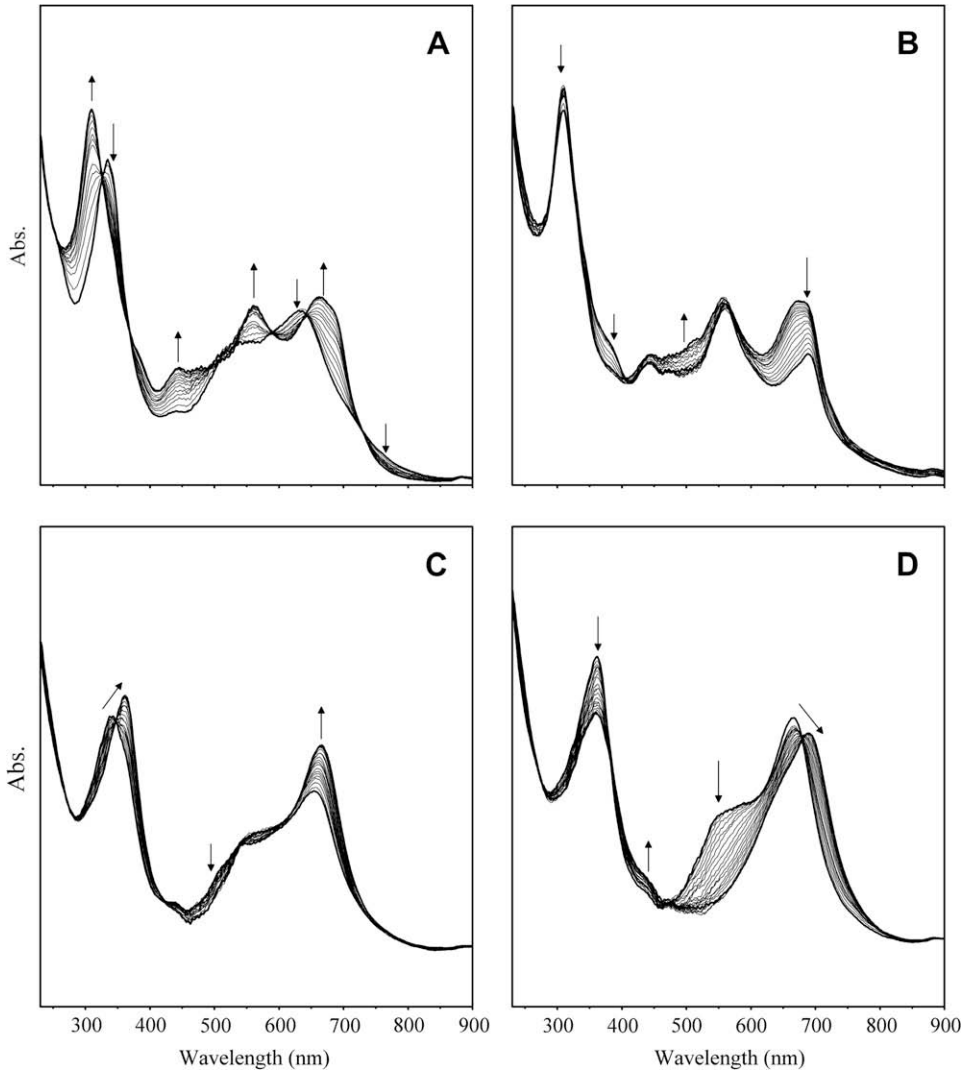

Fig. 7. In situ UV–vis spectral changes of **5**. (A) $E_{app} = -0.25$ V; (B) $E_{appp} = -1.20$ V; (C) $E_{app} = 0.90$ V; (D) $E_{app} = 1.65$ V.

showed the reversibility of R_1 and R_2 processes with approximately same slopes of the Cottrell lines representing the two potential steps of the processes.

4. Conclusion

The elemental analysis, IR, ^{1}H NMR, UV–vis data characterized the new compounds, porphyrazines (M = H, Mg, Zn and Co) with 2,3-dicyano-5-phenyl-5,6-dihydro-1,4-dithiin group fused to each pyrrole unit. Voltammetric and spectroelectrochemical characterizations of the metallo-porphyrazines (M = $2H^+$, Mg^{2+}, Zn^{2+} and Co^{2+}) substituted with 2,3-dicyano-5-phenyl-5,6-dihydro-1,4-dithiin groups on the peripheral positions are described. Voltammetric and spectroelectrochemical measurements show that the cobalt complex shows metal-based and ligand-based redox processes, while free, magnesium, and zinc porphyrazines give only ligand-based electron transfer processes. Analysis of the peaks recorded on CV and DPV indicates diffusion controlled reversible one-electron transfer characters of the redox processes. The electron releasing 2,3-dicyano-5-phenyl-5,6-dihydro-1,4-dithiin groups cause negative shifting of electron transfer processes when they compared with the common porphyrazine derivatives. Investigation of the solution redox processes provide deciding potential application of the complexes in related technological fields, such as electrochromism, data storage, and electrocatalyst. Observation of multi-electron, reversible, diffusion controlled reduction processes at less negative potentials indicates the possible technological usage of the complexes as electrocatalyst for the reduction of the various target species such as H^+, O_2, and CO_2. Different colors of the oxidized and reduced form of the complexes represent the possible usage of the complexes in solvatochromic or electrochromic applications.

Acknowledgements

This work was supported by the Research Fund of the Yildiz Technical University (Project no: 25-01-02-01).

References

[1] Luk'yanets EA. Mol Mater 1992;1:209.
[2] Bekaroğlu Ö. J Porphyrins Phthalocyanines 2000;4:465.
[3] Sanchez M, Chap N, Cazaux JB, Meunier B. Eur J Inorg Chem 2001:1775.
[4] Ahcar BN, Jayasree PK. Synth Met 2000;114:219.
[5] Karadeniz H, Gök Y, Kantekin H. Dyes Pigments 2007;75:498.
[6] Koçak M, Cihan Aİ, Okur A, Gül A, Bekaroğlu Ö. Dyes Pigments 2000;45:9.
[7] Sesalan BŞ, Koca A, Gül A. Polyhedron 2003;22:3083.
[8] Öztürk R, Gül A. Tetrahedron Lett 2004;45:947.
[9] Hasanov B, Gül A. Synth React Inorg Met Org Chem 2001;31:673.

[10] Öztürk R, Güner S, Aktaş B, Gül A. Synth React Inorg Met Org Chem 2001;31:1623.
[11] Polat M, Gül A. Dyes Pigments 2000;45:195.
[12] Uslu RZ, Gül A. CR Acad Sci Paris Ser II C Chim 2000;3:643.
[13] Akkuş H, Gül A. Transit Met Chem 2001;26:689.
[14] Sağlam Ö, Gül A. Polyhedron 2001;20:269.
[15] Leznoff CC, Lever ABP, editors. Phthalocyanines: properties and applications, vol. 1–4. New York: VCH Publishers; 1989–1996.
[16] Lever ABP, Pickens SR, Minor PC, Licoccia S, Ramaswany BS, Magnell K. J Am Chem Soc 1981;103:6800.
[17] Koca A, Özkaya AR, Selçukoğlu M, Hamuryudan E. Electrochim Acta 2007;52:2683.
[18] Kadish KM, Smith KM, Guilard R, editors. The porphyrin handbook, vol. 9. New York: Academic Press; 2000. p. 1–219.
[19] Bergami C, Donzello MP, Monacelli F, Ercolani C, Kadish KM. Inorg Chem 2005;44(26):9862.
[20] Donzello MP, Agostinetto R, Ivanova SS, Fujimori M, Suzuki Y, Yoshikawa H, et al. Inorg Chem 2005;44(23):8539.
[21] Bahr G, Schleitzer G. Chem Ber 1967;10:8.
[22] Simmons HE, Blomstrom DC, Vest RD. J Am Chem Soc 1962;84:4772.
[23] Simmons HE, Blomstrom DC, Vest RD. J Am Chem Soc 1962;84:4782.
[24] Kobayashi N. In: Kadish KM, Smith KM, editors. The porphyrin handbook, vol. 2. New York: Academic Pres; 2000. p. 301.
[25] Lelj F, Morelli G, Ricciardi G, Roviello A, Sirigu A. Liq Cryst 1992;12:941.
[26] Kobayashi N. In: Leznoff CC, Lever ABP, editors. Phthalocyanines properties and applications, vol. 2. New York: VCH; 1993. p. 104.
[27] Donzello MP, Dini D, D'Arcangelo G, Ercolani C, Zhan RQ, Ou ZP, et al. J Am Chem Soc 2003;125(46):14190.
[28] Koca A, Gonca E, Gül A. J Electroanal Chem 2008;612:231.
[29] Yarasir MN, Kandaz M, Koca A, Salih B. J Phys Chem C 2007;111:16558.
[30] Koca A, Şahin M, Gül A, Uslu RZ. Monatsh Chem 2002;133:1135.
[31] Koca A, Ö.Sağlam G, Gül A. Monatsh Chem 2003;134:11.
[32] Kissinger PT, Heineman WR. Laboratory techniques in electroanalytical chemistry. 2nd ed. New York: Marcel Dekker; 1996.
[33] Bard AJ, Faulkner LR. Electrochemical methods: fundamentals and applications. 2nd ed. New York: Wiley; 2001.
[34] Obirai J, Nyokong T. Electrochim Acta 2005;50:3296.
[35] Matlaba P, Nyokong T. Polyhedron 2002;21:2463.
[36] Obirai J, Nyokong T. Electrochim Acta 2005;50:5427.
[37] Koca A, Dinçer HA, Çerlek H, Gül A, Koçak MB. Electrochim Acta 2006;52:1199.